Integrated force and displacement sensing in active microcantilevers for off-resonance tapping mode atomic force microscopy

Natã F. S. de Bem[1], Michael G. Ruppert[1] Yuen K. Yong[1] and Andrew J. Fleming[1]

***Abstract*— Integrated on-chip actuation and sensing in microcantilevers for atomic force microscopy (AFM) allows faster scanning speeds, cleaner frequency responses and smaller cantilevers. However, a single integrated sensor suffers from cross-coupling between displacements originating from tip-sample forces and direct actuation. This paper addresses this issue by presenting a novel microcantilever with on-chip actuation and integrated dual sensing for AFM with application to off-resonance tapping modes in AFM. The proposed system is able to measure tip force and deflection simultaneously. A mathematical model is developed for a rectangular cantilever to describe the system and is validated with finite element analysis.**

I. INTRODUCTION

Since its invention, the atomic force microscope has been an indispensable tool for the investigation of small features. The atomic force microscope first generated topographic images [1] but later progressed to include mechanical properties [2] and chemical composition [3] which have found application in chemistry [4] and nanomanipulation [5]. During imaging, the microcantilever tip is positioned in close proximity to the sample which results in an interaction force that proportionally deflects the cantilever [6]. The sample is moved by a nanopositioner in patterns, such as raster or other trajectories [7]–[9].

The atomic force microscope has several modes of operation, with constant-amplitude intermittent-contact mode (also called Tapping Mode^{TM}) being the most widely used for interrogating soft samples [10]. A recent development for atomic force microscopy (AFM) is the so called off-resonance tapping (ORT) mode [11], introduced by Su et al. [12]. In this mode, the cantilever is excited at a frequency well below its resonance frequency [13]–[15], where the cantilever response is dominated by the static stiffness [15].

As the cantilever oscillates in ORT mode, it approaches and withdraws from the sample, generating force-distance curves at each cycle of interaction [14], [15]. Using the force-distance curves obtained at every cycle, a maximum interaction force is set as the control parameter for ORT, thus limiting the peak force between tip and sample [13]. Limiting the maximum interaction force makes ORT suitable for imaging soft, fragile samples, such as living cells or organisms [13], [14].

The common instrumentation interface for dynamic and ORT AFM consists of a piezoelectric shaker and/or a three degree-of-freedom nanopositioner and an optical beam deflection (OBD) system. Conventional methods either move the scan head or the sample using the nanospositioner in the vertical direction [16], [17] (Fig. 1 (a)). Due to the low resonance frequency of the nanopositioner, the vertical positioning bandwidth is limited to tens of Hertz [18]. Base excitation is yet another technique used in AFM, typically for dynamic modes. However, base excitation 1) introduces additional structural modes ("forest of peaks") that temper with the task of identifying the cantilever's flexural modes and 2) display low gain at low frequencies (Fig. 2 (a)) [16], [20]. Additionally, the motion of the cantilever base is not negligible at frequencies away from its resonance frequency [21] and, therefore, base excitation is not commonly used in ORT. Direct excitation of the cantilever is an alternative method that bypasses the slow mechanical bandwidth of the nanopositioner while being compatible with ORT. Several direct actuation techniques have been developed, including

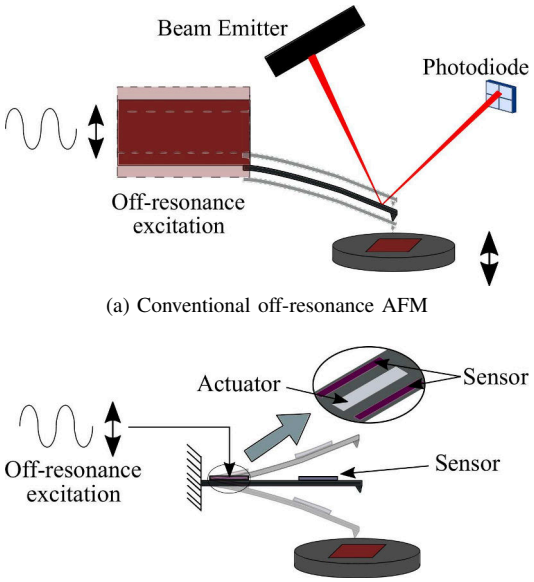

(a) Conventional off-resonance AFM

(b) Proposed off-resonance AFM system

Fig. 1: Schematic setup of an AFM operating in off-resonance tapping mode. (a) Conventional setup where the tapping motion is achieved by moving the entire cantilever head or sample using the nanopoisitioner and an OBD system is used to detect displacement. (b) Proposed setup for off-resonance tapping where the tapping motion is achieved with integrated actuation and a dual arrangement of integrated sensors measure the displacement and tip force.

[1]Natã F. S. de Bem, Michael G. Ruppert, Yuen K. Yong and Andrew J. Fleming are with the School of Electrical Engineering and Computer Science, University of Newcastle, Callaghan, Australia Natan.Franco@uon.edu.au

978-1-7281-9349-6/20/$31.00 ©2020 IEEE

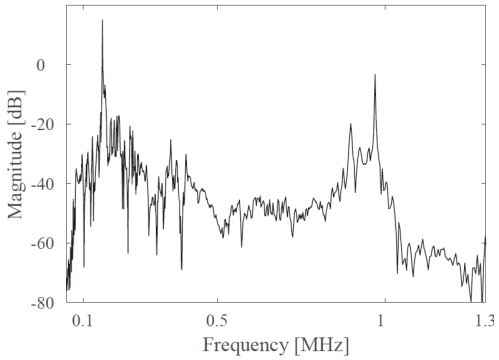

(a) Base excitation frequency response

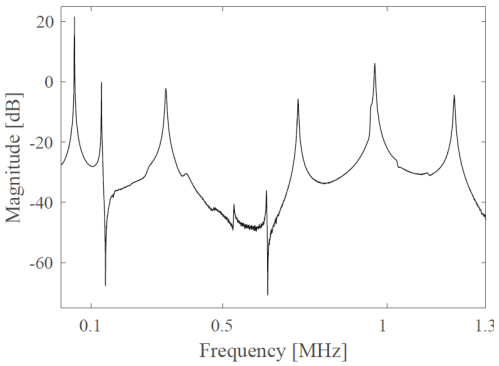

(b) Integrated on-chip actuation frequency response

Fig. 2: Frequency response of a cantilever driven at its (a) base and (b) self-excited using piezoelectric actuation [22].

photothermal [13] and piezoelectric [16]. Photothermal excitation has been reported [13], [17] in conjunction with ORT mode. This direct excitation method allows force-distance curves to be obtained up to two orders of magnitude faster than conventional methods [17]. However, photothermal excitation requires an additional laser beam, and the induced heat at the cantilever can damage sensitive samples [23]. Piezoelectric cantilevers are an alternative to the previous methods, providing benefits such as a smaller footprint and compatibility with off-the-shelf micro fabrication processes.

Almost all commercial AFM systems employ an OBD sensor to measure the displacement of the cantilever [16], with a resolution down to subnanometers [24]. However, the full width of the focused spot is typically a few micrometers, which limits the minimum width of the cantilever to tens of micrometers [25]. It has been shown that smaller cantilevers display higher resonance frequencies, which translates to a higher scanning speed, and increased sensitivity to smaller forces compared to larger cantilevers with the same stiffness [26]. Integrated sensing is an alternative to the traditional OBD method as it allows for the miniaturization of the cantilever. It exhibits a higher noise density compared to the OBD system [27], but it allows for parallel imaging, and for imaging light-sensitive samples under environments with low or varying optical transparency [25]. Integrated sensing mechanisms include: piezoelectric [22], capacitive [28], and piezoresistive [29].

The use of integrated on-chip actuation alongside integrated sensing offers the advantages of both techniques, i.e., faster scanning speed and smaller cantilevers [27], [30]. The main drawback of cantilevers with integrated on-chip actuation and sensing is the cross-coupling between displacements induced by direct actuation and tip-sample forces [31], [32]. This article describes a novel cantilever with on-chip actuation and two integrated sensors for use in ORT mode. The dual configuration of the sensors allows for the displacement and tip force to be measured, therefore addressing the cross-coupling issue of single integrated sensors. The cantilever has two piezoelectric sensors and a piezoelectric actuator. Piezoelectric material was chosen as it naturally generates charge under strain which is useful for sensing and it generates bending when a voltage is applied, which enables integrated actuation [33]; piezoelectric materials are also compatible with MEMS devices for silicon cantilevers [34].

II. MATHEMATICAL MODELING

Consider a rectangular cantilever made of a homogeneous, isotropic material with two piezoelectric sensors and one actuator, as shown in Figure 3. The thickness of the piezoelectric sensors are negligible. The actuator is at the base to maximize bending. The displacements along the x- and y-axes are small and are neglected in the model. The piezoelectric actuator generates bending due to the strain induced when a voltage is applied at its electrodes and the sensors generate a surface charge when a strain is induced in the cantilever when it is displaced. To minimize feedthrough between the sensor at the base and the actuator, a guard trace is placed around the piezoelectric actuator [35]. The cantilever is excited by a voltage applied at the piezoelectric actuator as well as a tip force acting on the free-end of the cantilever, generating bending. The charge generated by both sensors are the outputs of the system.

A. Piezoelectric Equations

Piezoelectric materials can be modeled following the IEEE Standard on Piezoelectricity as [33]

$$\varepsilon_1 = S_{13}^E \sigma_3 + d_{31} E_3, \quad (1)$$

$$D_3 = d_{31} \sigma_1 + \xi_{13}^\sigma E_3, \quad (2)$$

where (1) is used for actuation and (2) for sensing. The variables ε is the strain vector $[m/m]$, S is the compliance coefficients matrix $[m^2/N]$, σ is applied stress $[N/m^2]$, d is the piezoelectric strain constants $[m/V]$, E is the applied electric field $[V/m]$, D is the electric displacement vector $[C/m^2]$ and ξ is the permittivity matrix $[F/m]$.

For a piezoelectric actuator, the surface strain due to a voltage V_p applied is [33],

$$\varepsilon(z) = (k_\alpha z)\frac{d_{31} V_p}{t_p}, \quad (3)$$

where z is the position along the z-axis, d_{31} is the strain constant of the actuator and k_α is a constant that is related to the thickness and Young's modulus of the cantilever (t_c and

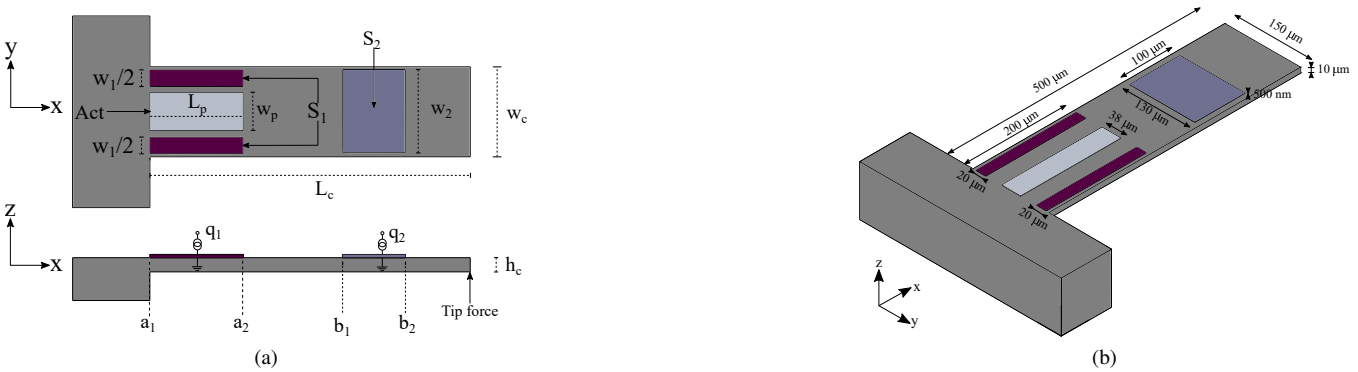

Fig. 3: (a) Schematic of the proposed cantilever design. The actuator has a fixed start position at the base ($x = 0$), while the sensors can be placed anywhere along the x-axis. (b) Proposed cantilever system. Due to manufacturing constraints, a space is required between the piezoelectric actuator and sensor. The actuator is centered to generate a symmetric bending.

E_c, respectively) and the actuator (t_p and E_p, respectively) by

$$k_\alpha = \frac{6E_cE_pt_ct_p\left(t_c+t_p\right)}{E_c^2t_c^4+E_cE_p\left(4t_c^3t_p+6t_c^2t_p^2+4t_ct_p^3\right)+E_p^2t_p^4}. \tag{4}$$

If the width of the actuator is not the same as the cantilever, (3) can be modified to

$$\varepsilon(z) \quad = \quad (k_\alpha z)\frac{d_{31}V_p}{t_p}\left(\frac{w_p}{w_c}\right), \tag{5}$$

where w_p/w_c represents the ratio between the width of the actuator and the cantilever.

For a piezoelectric sensor, the charge generated on its surface can be written as

$$q = d_{31}w_sE_s\int_{x_1}^{x_2}\varepsilon(z)dx, \tag{6}$$

where w_s is the width of the sensor and E_s is the Young's modulus of the sensor.

B. Piezoelectric Actuation Induced Bending

Considering the Euler-Bernoulli equation for a static cantilever

$$\frac{d^2}{dx^2}\left[E_rI_r\frac{d^2u_z}{dx^2}\right] = F_z(x), \tag{7}$$

where E_r and I_r are the Young's modulus and second moment of area of the cantilever, respectively, u_z is the displacement along the z-axis and F_z is a force applied along the z-axis. One can solve (7) based on the boundary conditions of the system. The displacement and slope at the base and the shear force at the tip are zero. The moment

$$M = -E_rI_r\frac{\varepsilon}{z}, \tag{8}$$

is constant where the actuator is located ($0 \le x \le L_p$) and zero elsewhere ($L_p < x \le L_c$).
Solving the Euler-Bernoulli equation for the aforementioned boundary conditions and using (5) and (7) results in

$$u_z(x) = \begin{cases} \frac{k_\alpha d_{31}}{2t_p}\frac{w_p}{w_c}V_px^2, & \text{for } 0 \le x \le L_p \\ \frac{k_\alpha d_{31}}{2t_p}\frac{w_p}{w_c}V_pL_p\left(2x-L_p\right), & \text{for } L_p < x \le L \end{cases}, \tag{9}$$

where L_p is the length of the actuator, starting at $x = 0$. The displacement for the cantilever due to a piezoelectric actuation is composed of a set of two equations that describe the displacement where the piezoelectric actuator is located ($0 \le x \le L_p$) and elsewhere ($L_p < x \le L_c$). The tip displacement of the cantilever due to a voltage applied at the actuator, d_V, can be stated as

$$d_V = \frac{k_\alpha d_{31}}{2t_p}\frac{w_p}{w_c}V_pL_p\left(2L_c-L_p\right). \tag{10}$$

The generated surface charge on the sensor depends on the induced surface strain as shown in (6), which can be expressed as

$$\varepsilon = \frac{d^2u_z}{dx^2}. \tag{11}$$

Because the equation that describes the displacement of the cantilever is of first order for $L_p < x \le L_c$, the strain and hence charge generated by the sensor will be zero. For $0 \le x \le L_p$, a second order equation describes the displacement of the cantilever, which results in a constant strain and the charge can be stated as

$$q \quad = \quad d_{31}^2b_sE_s(k_\alpha z)\frac{1}{t_p}\frac{w_p}{w_c}V_p(x)\Big|_{x_1}^{x_2} \tag{12}$$

where the actuator is located and depends directly on the length of the sensor. Therefore,

$$q_{1V} = d_{31}^2w_1E_s\left(k_\alpha z+k_\varepsilon\right)\frac{V_p}{t_p}\frac{w_p}{w_c}\left(a_2-a_1\right) \tag{13}$$

and

$$q_{2V} = 0. \tag{14}$$

C. Tip Force Induced Bending

The tip displacement in response to an applied tip force can be derived similarly using (7). For the case of a tip force acting on the cantilever, the displacement and slope at its base are zero, as well as the moment on its free-end. The shear force at the tip is equal to the tip force applied.

Solving for these boundary conditions, the displacement of the cantilever can be stated as

$$u_z(x) = \frac{1}{6E_rI_r}F_t\left(-x^3+3L_cx^2\right). \tag{15}$$

The tip displacement can be expressed as

$$d_F = \frac{L_c^3}{3E_rI_r}F_t, \tag{16}$$

where d_F is the tip displacement due to a tip force, F_t.

Based on (6) and (15), the surface charge of a sensor due to a tip force is

$$q = -\frac{zd_{31}b_s}{2I_r}\frac{E_s}{E_r}F_t\left(-x^2+2L_cx\right)\Big|_{x_1}^{x_2}. \tag{17}$$

Therefore,

$$q_{1F} = -\frac{zd_{31}w_1}{2I_r}\frac{E_s}{E_r}F_t\left(-\left(a_2^2-a_1^2\right)+2L_c(a_2-a_1)\right) \tag{18}$$

and

$$q_{2F} = -\frac{zd_{31}w_2}{2I_r}\frac{E_s}{E_r}F_t\left(-\left(b_2^2-b_1^2\right)+2L_c\left(b_2-b_1\right)\right). \tag{19}$$

The highest strain is at the base ($x = 0$) and its value decreases up to the tip ($x = L$), where it is zero. As shown by (17), the generated charge depends on the integral of the induced strain at the piezoelectric layer, therefore, the sensor should be placed as close to the base and be chosen as long as possible. The sensor located parallel to the piezoelectric actuator generates charge due to both inputs, i.e. actuation and tip force, while the sensor placed away from the actuator has its generated charge dependent only on the tip force.

D. Surface Charge as a function of Tip Displacement and Tip Force

The total tip displacement, d_T, is defined as the sum of the displacement due to the tip force and the piezoelectric actuator and using (10) and (16) is given by

$$d_T = \frac{k_\alpha d_{31p}}{2t_p}V_p\frac{w_p}{w_c}L_p\left(2L_c-L_p\right)+\frac{L^3}{3E_rI_r}F_t, \tag{20}$$

The total charge generated by sensor 1 is given by the charge generated due to the piezoelectric actuator, q_{1V}, and tip force, q_{1F}. Therefore,

$$\begin{aligned} q_1 &= d_{31}^2w_1E_s\left(k_\alpha z+k_\varepsilon\right)\frac{V_p}{t_p}\frac{w_p}{w_c}\left(a_2-a_1\right) \\ &-\frac{zd_{31}w_1}{2I_r}\frac{E_s}{E_r}F_t\left(-\left(a_2^2-a_1^2\right)+2L_c\left(a_2-a_1\right)\right). \end{aligned} \tag{21}$$

The total charge at sensor 2 due to the piezoelectric actuator, q_{2V} and tip force, q_{2F}, is

$$q_2 = -\frac{zd_{31}w_2}{2I_r}\frac{E_s}{E_r}F_t\left(-\left(b_2^2-b_1^2\right)+2L_c\left(b_2-b_1\right)\right). \tag{22}$$

(20) shows the total tip displacement of a cantilever due to a piezoelectric actuator and tip force and replacing it in (21), results in

$$\begin{aligned} q_1 &= \frac{2d_{31}w_1E_sz}{L_p\left(2L-L_p\right)}\cdot\left(d_T-\frac{L^3}{3E_rI_r}F_t\right)\left(a_2-a_1\right) \\ &-\frac{zd_{31}w_1}{2I_r}\frac{E_s}{E_r}F_t\left(-\left(a_2^2-a_1^2\right)+2L\left(a_2-a_1\right)\right) \end{aligned}, \tag{23}$$

which relates the charge generated at sensor 1 to tip displacement and tip force. Using (22) and (23) for the generated charge for both sensors and inverting them so that the outputs are tip force and tip displacement, yields

$$F_t = -\frac{2E_rI_r}{E_sw_2d_{31}z\left(b_1-b_2\right)\left(b_1+b_2-2L_c\right)}q_2 \quad , \tag{24}$$

and

$$\begin{aligned} d_T &= \left(\frac{L_p\left(2L_c-L_p\right)}{2E_sw_1d_{31}\left(a_1-a_2\right)}\right)q_1 \\ &+\left(\frac{2L_c^3-3zL_p\left(2L_c-L_p\right)\left(a_1+a_2-2L_c\right)}{3E_sw_2d_{31}z\left(b_1-b_2\right)\left(b_1+b_2-2L_c\right)}\right)q_2 \end{aligned}. \tag{25}$$

Rewriting Equations (24) and (25) in matrix form results in

$$\begin{bmatrix} d_T \\ F_t \end{bmatrix} = \begin{bmatrix} k_{11} & k_{12} \\ 0 & k_{22} \end{bmatrix}\cdot\begin{bmatrix} q_1 \\ q_2 \end{bmatrix}, \tag{26}$$

where the constants k_{11}, k_{12} and k_{22} depend only on physical parameters. (26) introduces a matrix to calculate a tip displacement and force knowing the generated charge from the two piezoelectric sensors, taking into account the influence of a piezoelectric actuator.

III. FINITE ELEMENT ANALYSIS

Finite element analysis (FEA) was used to validate the mathematical model. The FEA was modeled using ANSYS Workbench and the PiezoAndMEMS extension. The dimensions of the cantilever system are shown in Fig. 3. All piezoelectric transducers are 500 nm thick. A voltage of 10 V is applied at the actuator and a tip force of 100 nN is applied on the free-end of the cantilever.

The strain is concentrated where the actuator is located (Fig. 4 (a)), and when a tip force is applied, the strain gradually decreases along the x-axis (Fig. 4 (b)). Figure 5 shows the strain along the x-axis of the surface of the cantilever for the finite element (FE) model, in blue, and the mathematical model, in red. In (a), the cantilever is under a piezoelectric actuation and in (b), under a tip force. Points A-G are computational errors due to differentiation at discontinuities [36]. In the mathematical model, the strain induced by the actuator is zero outside of the piezoelectric boundaries. However, the FEA results indicate that the induced strain in sensor 2 due to the piezoelectric actuator is equivalent to 0.5% of the strain in sensor 1 (Table I (a)). This small cross-coupling induces a strain at sensor 2 of the same order of magnitude as the strain due to a tip force due to the small forces being detected (100 nN). Therefore, in the scope of the defined mathematical model, the previous assumption is plausible. The inset C (Fig. 5 (a)) shows that there is an induced strain in the cantilever in the areas outside the piezoelectric actuator boundaries, but its magnitude is much lower than the strain in the region between points A and B. In real devices, the strain will not instantaneously cease, and thus a small remaining strain is expected [37] and can be minimized by placing sensor 2 further from the actuator. Although the charges generated by sensors 1 and 2 due to a tip force display higher difference comparing FEA and

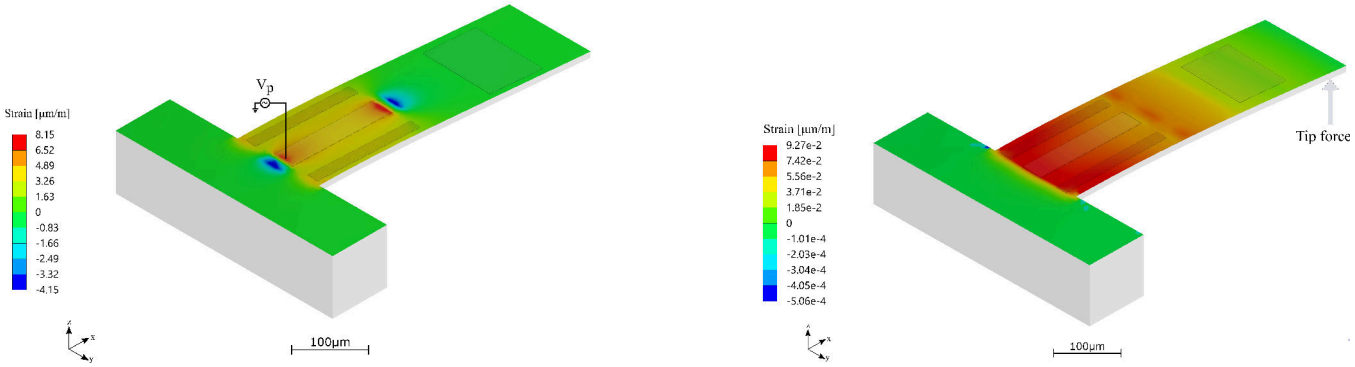

(a) Surface strain due to piezoelectric actuation

(b) Surface strain due to a tip force

Fig. 4: Strain distribution at the surface of the cantilever under (a) piezoelectric actuation of 10 V and (b) tip force of 100 nN.

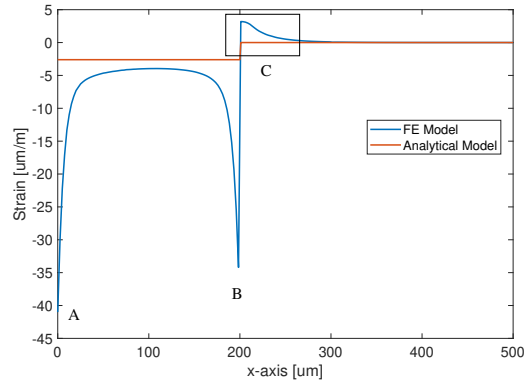

(a) Strain due to a piezoeletcric actuation of 10 V.

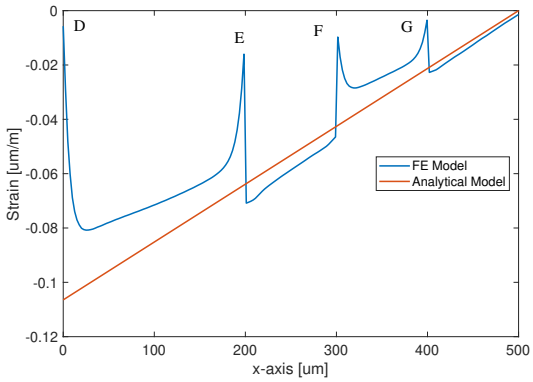

(b) Strain due to a tip force of 100 nN.

Fig. 5: Surface strain profile along the x-axis for the cantilever system for (a) piezoelectric actuation and (b) tip force.

the mathematical model, it should be noted that the absolute difference is $\sim$ 0.1 fC for both sensors. Another factor that can influence the generated charge are the singularities at the boundary of the piezoelectric regions (Fig. 5).

IV. CONCLUSIONS

Integrated on-chip actuation allows a much faster vertical positioning bandwidth in off-resonance tapping modes, while integrated sensing makes smaller cantilevers feasible. Smaller cantilevers are of particular interest as they allow for faster scanning speed due to their higher resonant frequencies, whilst maintaining relatively low stiffness. Improving the scanning speed in AFM allows rapidly changing samples and processes to be recorded, while a higher sensitivity to interatomic forces can reduce damage during the scan. The proposed system is capable of acquiring both, an estimate for the tip force and deflection simultaneously. Moreover, the dual sensing configuration allows the cross-coupling between actuator and sensors to be identified and compensated.

Placing sensor 2 further from the actuator diminishes this discrepancy at the cost of sensitivity to tip forces. Moreover, the mathematical model simplifies the system to one dimension, which results in straightforward equations. An improved mathematical model will be investigated to account for the piezoelectric layer and the other dimensions and the hysteresis effect in order to mitigate the difference on the generated charges between the two models.

TABLE I: Tip displacement, induced strain and generated charge comparison between FE Model and analytical (AN) model for a rectangular cantilever due to (a) piezoelectric actuation and (b) tip force.

(a)

Measurement	AN Model	FE Model	Error (%)
Tip displacement [nm]	37.915	42.23	11.38
Avg strain Sensor 1 [μm/m]	-2.606	-3.04	16.65
Avg strain Sensor 2 [μm/m]	0.00	0.015	-
Charge at Sensor 1 [fC]	-15.39	-15.95	3.64
Charge at Sensor 2 [fC]	0.00	-0.386	-

(b)

Measurement	AN Model	FE Model	Error (%)
Tip displacement [nm]	1.613	1.742	8.00
Avg strain Sensor 1 [μm/m]	-0.085	-0.077	9.41
Avg strain Sensor 2 [μm/m]	-0.032	-0.024	25.00
Charge at Sensor 1 [fC]	-0.503	-0.422	16.10
Charge at Sensor 2 [fC]	-0.306	-0.190	37.91

Currently, four different designs of the cantilever system are being manufactured by MEMSCAP®. These designs display different characteristics such as stiffness, resonance frequency and sensor size. Future work includes the characterization of the manufactured devices, including their force and displacement sensitivity. Based on the mathematical model presented, the position and shape of the sensors will be further optimized.

REFERENCES

[1] L. Zhou, M. Cai, T. Tong, and H. Wang, "Progress in the correlative atomic force microscopy and optical microscopy," *Sensors*, vol. 17, no. 4, 2017.

[2] M. Radmacher, R. Tillmann, and H. Gaub, "Imaging viscoelasticity by force modulation with the atomic force microscope," *Biophysical Journal*, vol. 64, no. 3, pp. 735 – 742, 1993.

[3] D. Ebeling, B. Eslami, and S. D. J. Solares, "Visualizing the subsurface of soft matter: Simultaneous topographical imaging, depth modulation, and compositional mapping with triple frequency atomic force microscopy," *ACS Nano*, vol. 7, no. 11, pp. 10 387–10 396, 2013, pMID: 24131492.

[4] M. Jazvinšćak Jembrek, G. Simic, P. Hof, and S. Šegota, "Atomic force microscopy as an advanced tool in neuroscience," *Translational Neuroscience*, vol. 6, p. 117, 06 2015.

[5] D. Y. Abramovitch, S. B. Andersson, L. Y. Pao, and G. Schitter, "A tutorial on the mechanisms, dynamics, and control of atomic force microscopes," in *2007 American Control Conference*, July 2007, pp. 3488–3502.

[6] S. Ian Moore and Y. K. Yong, "Design and characterisation of cantilevers for multi-frequency atomic force microscopy," *Micro Nano Letters*, vol. 12, no. 5, pp. 315–320, 2017.

[7] Y. K. Yong, S. O. R. Moheimani, and I. R. Petersen, "High-speed cycloid-scan atomic force microscopy," *Nanotechnology*, vol. 21, no. 36, 2010.

[8] A. Bazaei, Y. K. Yong, and S. O. R. Moheimani, "Combining spiral scanning and internal model control for sequential afm imaging at video rate," *IEEE Transactions on Mechatronics*, vol. 22, no. 1, pp. 371–380, 2017.

[9] Y. K. Yong, A. Bazaei, and S. O. R. Moheimani, "Video-rate lissajous-scan atomic force microscopy," *IEEE Transactions on Nanotechnology*, vol. 13, no. 1, pp. 85–93, 2014.

[10] O. Sahin, S. Magonov, C. su, C. F Quate, and O. Solgaard, "An atomic force microscope tip designed to measure time-varying nanomechanical forces," *Nature nanotechnology*, vol. 2, pp. 507–14, 08 2007.

[11] W. Walczyk, P. M. Schön, and H. Schönherr, "The effect of PeakForce tapping mode AFM imaging on the apparent shape of surface nanobubbles," *Journal of Physics: Condensed Matter*, vol. 25, no. 18, p. 184005, apr 2013.

[12] S. Hu, L. Mininni, Y. Hu, N. Erina, J. Kindt, and C. Su, "High-speed atomic force microscopy and peak force tapping control," in *Metrology, Inspection, and Process Control for Microlithography XXVI*, A. Starikov, Ed., vol. 8324, International Society for Optics and Photonics. SPIE, 2012, pp. 576 – 585.

[13] A. P. Nievergelt, C. Brillard, H. A. Eskandarian, J. D. McKinney, and G. E. Fantner, "Photothermal off-resonance tapping for rapid and gentle atomic force imaging of live cells," *International Journal of Molecular Sciences*, vol. 19, no. 10, 2018.

[14] H. Schillers, I. Medalsy, S. Hu, A. L. Slade, and J. E. Shaw, "Peakforce tapping resolves individual microvilli on living cells," *Journal of Molecular Recognition*, vol. 29, no. 2, pp. 95–101, 2016.

[15] K. Xu, W. Sun, Y. Shao, F. Wei, X. Zhang, W. Wang, and P. Li, "Recent development of peakforce tapping mode atomic force microscopy and its applications on nanoscience," *Nanotechnology Reviews*, vol. 7, 09 2018.

[16] S. I. Moore, M. G. Ruppert, and Y. K. Yong, "Multimodal cantilevers with novel piezoelectric layer topology for sensitivity enhancement," *Beilstein Journal of Nanotechnology*, vol. 8, pp. 358–371, 2017.

[17] A. Nievergelt, N. Banterle, S. H. Andany, P. Gönczy, and G. Fantner, "High-speed photothermal off-resonance atomic force microscopy reveals assembly routes of centriolar scaffold protein sas-6," *Nature Nanotechnology*, vol. 13, 08 2018.

[18] Y. K. Yong, S. O. R. Moheimani, B. J. Kenton, and K. K. Leang, "Invited review article: High-speed flexure-guided nanopositioning: Mechanical design and control issues," *Review of Scientific Instruments*, vol. 83, no. 12, p. 121101, 2012. [Online]. Available: https://doi.org/10.1063/1.4765048

[19] C. S. S. H. H. Ma, "Method and apparatus of using peak force tapping mode to measure physical properties of a sample," Patent US9 291 640B2, 2016.

[20] M. G. Ruppert and S. O. R. Moheimani, "High-bandwidth multimode self-sensing in bimodal atomic force microscopy," *Beilstein Journal of Nanotechnology*, vol. 7, pp. 284–295, 2016.

[21] L. Costa and M. S. Rodrigues, "Influence of spurious resonances on the interaction force in dynamic afm," *Beilstein Journal of Nanotechnology*, vol. 6, pp. 420–427, 2015.

[22] M. G. Ruppert, S. I. Moore, M. Zawierta, A. J. Fleming, G. Putrino, and Y. K. Yong, "Multimodal atomic force microscopy with optimized higher eigenmode sensitivity using on-chip piezoelectric actuation and sensing," *Nanotechnology*, vol. 30, no. 8, p. 085503, jan 2019. [Online]. Available: https://doi.org/10.1088%2F1361-6528%2Faae40b

[23] D. Kiracofe, K. Kobayashi, A. Labuda, A. Raman, and H. Yamada, "High efficiency laser photothermal excitation of microcantilever vibrations in air and liquids," *The Review of scientific instruments*, vol. 82, p. 013702, 01 2011.

[24] K. M. Hansen and T. Thundat, "Microcantilever biosensors," *Methods*, vol. 37, no. 1, pp. 57 – 64, 2005, biosensors.

[25] M. Dukic, J. D Adams, and G. Fantner, "Piezoresistive afm cantilevers surpassing standard optical beam deflection in low noise topography imaging," *Scientific reports*, vol. 5, p. 16393, 11 2015.

[26] M. B. Viani, T. E. Schäffer, A. Chand, M. Rief, H. E. Gaub, and P. K. Hansma, "Small cantilevers for force spectroscopy of single molecules," *Journal of Applied Physics*, vol. 86, no. 4, pp. 2258–2262, 1999.

[27] M. G. Ruppert and S. O. R. Moheimani, "A novel self-sensing technique for tapping-mode atomic force microscopy," *Review of Scientific Instruments*, vol. 84, no. 12, p. 125006, 2013.

[28] J. Brugger, N. Blanc, P. Renaud, and N. de Rooij, "Microlever with combined integrated sensor/actuator functions for scanning force microscopy," *Sensors and Actuators A: Physical*, vol. 43, no. 1, pp. 339 – 345, 1994.

[29] J. Bausells, "Piezoresistive cantilevers for nanomechanical sensing," *Microelectronic Engineering*, vol. 145, pp. 9 – 20, 2015, micro/Nano Devices and Systems 2014 An open focused special thematic issue of Microelectronic Engineering.

[30] G. E. Fantner, W. Schumann, R. J. Barbero, A. Deutschinger, V. Todorov, D. S. Gray, A. M. Belcher, I. W. Rangelow, and K. Youcef-Toumi, "Use of self-actuating and self-sensing cantilevers for imaging biological samples in fluid," *Nanotechnology*, vol. 20, no. 43, p. 434003, oct 2009.

[31] Y.-S. Kim, H.-J. Nam, S.-M. Cho, J.-W. Hong, D.-C. Kim, and J. U. Bu, "Pzt cantilever array integrated with piezoresistor sensor for high speed parallel operation of afm," *Sensors and Actuators A: Physical*, vol. 103, no. 1, pp. 122 – 129, 2003.

[32] T. Michels, E. Guliyev, M. Klukowski, and I. W. Rangelow, "Micromachined self-actuated piezoresistive cantilever for high speed spm," *Microelectronic Engineering*, vol. 97, pp. 265 – 268, 2012, micro- and Nano-Engineering (MNE) 2011, selected contributions: Part I.

[33] S. O. Reza Moheimani and A. Fleming, *Piezoelectric Transducers for Vibration Control and Damping*, 01 2006.

[34] S. Tadigadapa and K. Mateti, "Piezoelectric mems sensors: State-of-the-art and perspectives," *Measurement Science and Technology*, vol. 20, p. 092001, 07 2009.

[35] M. G. Ruppert and Y. K. Yong, "Note: Guaranteed collocated multimode control of an atomic force microscope cantilever using on-chip piezoelectric actuation and sensing," *Review of Scientific Instruments*, vol. 88, no. 8, p. 086109, 2017. [Online]. Available: https://doi.org/10.1063/1.4990451

[36] W. Younis, "Chapter 9 - the stress analysis environment," in *Up and Running with Autodesk Inventor Simulation*, 2nd ed., W. Younis, Ed. Oxford: Butterworth-Heinemann, 2010, pp. 235 – 275.

[37] Z. Bi, "Chapter 12 - validation and verification," in *Finite Element Analysis Applications*, Z. Bi, Ed. Academic Press, 2018, pp. 455 – 494.